Robotics and Computer Integrated Manufacturing 58 (2019) 172–180

Contents lists available at ScienceDirect

Robotics and Computer Integrated Manufacturing

journal homepage: www.elsevier.com/locate/rcim

Full length Article

Optimization design for a compact redundant hybrid parallel kinematic machine

Yen Ping-Lang[a], Wang Ching-Heng[a], Lin Hao-Ting[b], Hung Shuo-Suei[c,d,*]

[a] Department of Biomechatronics Engineering, National Taiwan University, Taipei, Taiwan
[b] Department of Bio-Industrial Mechatronics Engineering, National Chung Hsing University, Taichung, Taiwan
[c] Department of Orthopedics, Taipei Tzu Chi Hospital, Buddhist Tzu Chi Medical Foundation, New Taipei City, Taiwan
[d] School of Medicine, Tzu Chi University, Hualien, Taiwan

ARTICLE INFO

Keywords:
Parallel kinematic machine
Hybrid mechanism
Redundant manipulator
Parameter optimization
Redundancy control

ABSTRACT

Designing a machine tool that simultaneously satisfies the requirements of high rigidity, large dexterous workspace and small footprint is challenging. This paper proposed a redundant hybrid manipulator as a machine tool with these features. The design attempted to integrate the advantages of a PKM (parallel kinematic mechanism), SKM (serial kinematic mechanism) and redundancy mechanism. The geometric parameters of the manipulator were elaborately tuned to overcome intrinsic and extrinsic singularities with an optimal machining plane. High-accuracy and complex-shape machine results have been experimentally verified. The advantage is the ability to shorten the required strokes of the linear actuators effectively. This change not only improves the performance in terms of rigidity, accuracy and dynamics of the entire mechanism but also reduces the cost of the materials and the performance ratio. The second is to decrease the overall machinery-footprint-to-workspace ratio and lower the manufacturing cost via occupied floor space reduction and layout flexibility of the production line.

1. Introduction

Five-axis machine tools are the most commonly equipped for arbitrary-shape machining purposes [1]. One of the classifications is based on their spatial structure and categorized into serial kinematic machines (SKMs), parallel kinematic machines (PKMs) and hybrid kinematic machines (HKMs). SKMs are the most popular type and feature kinematics and control simplicity. Massive mass is usually necessary for the links to provide stiffness, and the machining dynamics may subsequently be limited by the large inertias [2–4]. PKMs are particularly proposed for low ratios of strength-to-weight. A PKM is constructed by close-chains so that the tool is supported and actuated simultaneously by multi-limbs to accomplish highly dynamic performance [5–6]. However, the topology also suffers from its complex and small workspace, kinematic singularities and inconsistent dexterity. The large footprint of PKM also limits the installation flexibility in manufacturing layout [7–8]. Therefore, the issue of fulfilling all the requirements of accuracy, high rigidity, large dexterous workspace and small footprint-to-workspace ratio still remains for complex-shape machining purposes.

A hybrid structure of SKM and PKM emerged to leverage the advantages of both types of kinematics. Many combinations of mechanism structures have evolved, such as (1) PKM cascaded SKM [9], (2) PKM cascaded to SKM [10], (3) PKM and SKM separated to the gantry and base, respectively [11]. The HKM can also be classified by taking into account the machining functionalities, such as (1) the method of positioning the tool's translation and orientation using PKM or SKM [9] and (2) the mounting arrangement of tool and workpiece on PKM or SKM [12]. A hybrid structure generally improves both the footprint-to-workspace ratio and dynamic performance. However, the issues of dexterity and singularity avoidance still remain. Therefore, studies on utilizing either actuation or kinematic redundancy to improve the dexterity and singularity avoidance of PKMs have been presented [13]. Actuation redundancy is to actuate some of the existing passive joints in kinematic chains through sophisticated force control so that the stiffness of the end-effector and the force transmission of kinematic chains can be modulated [14–15]. Kinematic redundancy introduces an extra degree of freedom of the kinematic chain so that optimization in term of singularity avoidance can be accomplished [16–17]. The energy consumption could also be considerably reduced [18]. More solutions may be investigated in the aspects of topological variations or control strategies by regarding a parallel robot as a special case of multiple serial robot coordination [19]. Particularly soft computing techniques in

* Corresponding author.
E-mail address: hung_ortho@tzuchi.com.tw (S.-S. Hung).

https://doi.org/10.1016/j.rcim.2019.02.006
Received 30 August 2018; Received in revised form 5 December 2018; Accepted 23 February 2019
Available online 09 March 2019

recent year have shown promising results in kinematic control for energy consumption minimization of a redundant manipulator [20]. In summary, hybrid structure and redundancies are of high potential for elevating the overall performance of machine tools. However, the integrated investigation of maximizing the benefit of redundant axes combined with hybrid structure mechanism design for the above issues is still not completely addressed, such as (1) optimizing the footprint and limb inertia and (2) elimination of internal singularities related to ball joint design.

This paper proposes a gantry-type HKM with a vertical-axis (or *Z*-axis) redundancy. The HKM combines a 3-DOF PKM with a 3-DOF Cartesian SKM, where the tooling is mounted on the PKM and the workpiece on the SKM. The *Z*-axis redundancy on the SKM allows the PKM to operate on the optimal working plane where the maximal workspace can be obtained. Moreover, the ball joint was added with a compensation block, of which the mounting angle can be elaborately chosen to remove internal singularities. The kinematic parameters of limbs were optimized to meet the requirements to maximize the footprint-to-workspace ratio and minimize the limb size. The concept was verified by a prototype for machining a workpiece with free curve. The remainder of the paper is organized as follows: (1) description of the overall mechanism structure; (2) kinematic model for singularity analysis; (3) optimization of the link and joint parameters to maximize the workspace; (4) redundancy controller design; and (5) verification by simulation and experiment.

2. Overall structure

The hybrid redundant manipulator is composed of a 3-DOF PKM and 3-DOF SKM (Fig. 1). The 6-DOF manipulator is arranged with 1-DOF redundancy in the *Z*-axis for 5-axis machining purposes. The 3-DOF PKM is of RPS type with a linear actuator on each limb, and the 3-DOF SKM is with a linear actuator in the *X*-, *Y*-, and *Z*-axis, respectively. The spindle is mounted on the moving platform of the PKM, whereas the workpiece is on the counterpart of the SKM. The PKM's base is fixed to the gantry of the SKM's base. The hybrid redundant manipulator performs the rotational motions in the *C*-axis and *A*-axis independently via PKM and the translational motion in the *X, Y* and *Z*-axis via the PKM and SKM together.

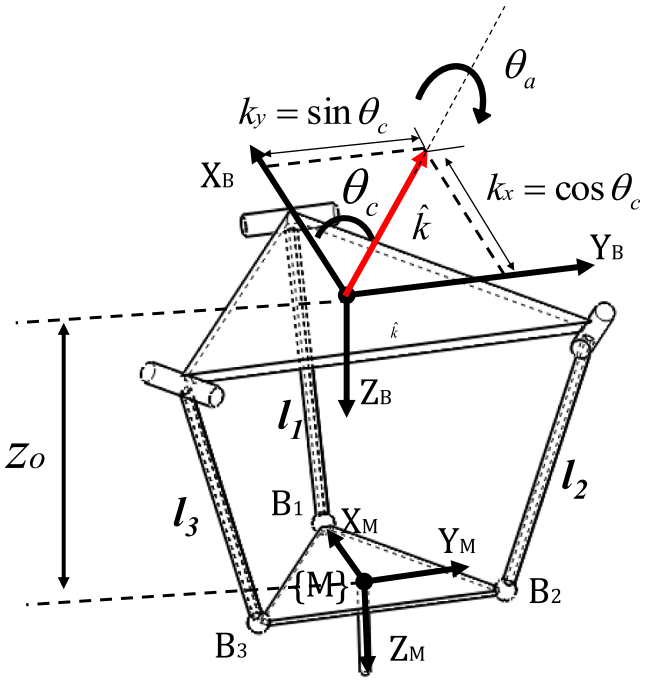

Fig. 2. Schematic of the PKM kinematics.

2.1. Kinematics of the PKM

The RPS-PKM (Fig. 2) consists of a base {B}, a moving platform {M} and three connected linear actuators $\{L\} = \{(l_1, l_2, l_3)^T\}$. The tool pose

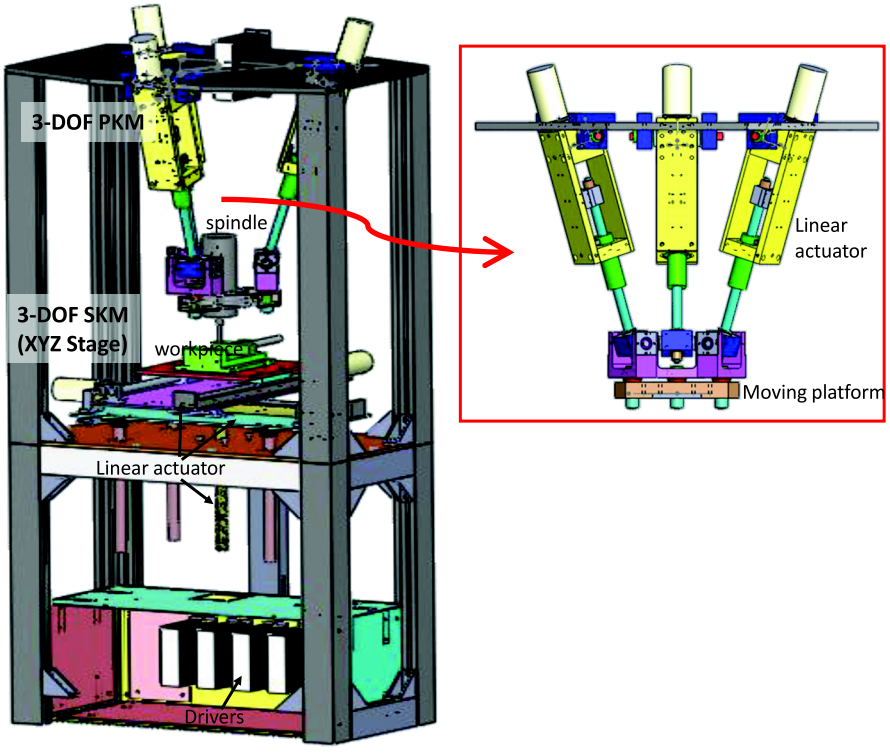

Fig. 1. Schematic of the hybrid redundant machine tool.

${}^{B}_{M}T$ is derived to associate with the linear actuator variables $(l_1, l_2, l_3)^T$ as follows. Let ${}^{B}_{M}T = \begin{bmatrix} R_{\hat{k},\theta} & P_m \\ 0 & 1 \end{bmatrix}$, where $R_{\hat{k},\theta}$ is the orientation of the tool relative to the base frame, $\hat{k} = [k_k, k_y, k_z]^T$ is the rotation axis, , $\theta = \theta_a$ is the rotation angle, $P_m = [X_m, Y_m, Z_m]^T$ is the translational vector, $x_m = -0.5r((c^2\theta_c - s^2\theta_c)(c\theta_a - 1))$, and $y_m = r((c\theta_c s\theta_c)(c\theta_a - 1))$. There are only three independent variables associated with the tool pose ${}^{B}_{M}T$. The inverse kinematic function is described as:

$$q = f_p(x) \tag{1}$$

and the relationship between the Cartesian variable $x = \begin{bmatrix} z_m \\ \theta_c \\ \theta_a \end{bmatrix}$ and the joint variable $q = \begin{bmatrix} l_1 \\ l_2 \\ l_3 \end{bmatrix}$ can be explicitly derived as Eqs. (2)–(4).

$$l_1 = \frac{\mathrm{R} + \mathrm{r}(c^2\theta_c - s^2\theta_c)(c\theta_a - 1)}{2} - \mathrm{r}(c\theta_a - c\theta_c{}^2(c\theta_a - 1)^2) + \sqrt{(z_m - \mathrm{r}s\theta_a s\theta_c)^2} \tag{2}$$

$$l_2 = \frac{1}{2}\sqrt{\left(z + \frac{\mathrm{r}s\theta_a s\theta_c}{2} + \frac{\sqrt{3}\,\mathrm{r}c\theta_c s\theta_a}{2}\right)^2 + \frac{(\sqrt{3}\,\mathrm{r}c\theta_a s^2\theta_c(c\theta_a - 1) - \sqrt{3}R + 3rc\theta_c s\theta_c(c\theta_a - 1))^2}{4} + ((r(c^2\theta_c - s^2\theta_c) + rc\theta_a - rc^2\theta_c + \sqrt{3}\,rc\theta_c s\theta_c)(c\theta_a - 1) - R)^2} \tag{3}$$

$$l_3 = \frac{1}{2}\sqrt{\left(z + \frac{\mathrm{r}s\theta_a s\theta_c}{2} + \frac{\sqrt{3}\,\mathrm{r}c\theta_c s\theta_a}{2}\right)^2 + \frac{(\sqrt{3}\,\mathrm{r}c\theta_a s^2\theta_c(c\theta_a - 1) - \sqrt{3}R + 3rc\theta_c s\theta_c(c\theta_a - 1))^2}{4} + \frac{((r(c^2\theta_c - s^2\theta_c) + rc\theta_a - rc^2\theta_c + \sqrt{3}\,rc\theta_c s\theta_c)(c\theta_a - 1) - R)^2}{4}} \tag{4}$$

2.2. Kinematic singularity analysis

The RPS-PKM singularities are divided into two categories: (1) boundary singularity and (2) intrinsic singularity. The boundary singularity is associated with the reachable workspace by the end-effector of the mechanism. The reachable workspace consists of all the poses of the end-effector poses that have real solutions l_1–l_3 from Eqs. (2)–(4) within the stroke range of linear actuators. Therefore, the size of the reachable workspace is dependent on the diameter ratio r/R of the moving and base platform and the stroke S of the linear actuators. Generally, a small diameter ratio r/R and large stroke S of the linear actuators lead to a large workspace.

The intrinsic singularity is associated with certain special postures, at which an additional degree of freedom occurs and rigidity is lost. The intrinsic singularity of a PKM can be found from the Jacobian of the kinematic equation. Taking the derivative of Eq. (1), we have:

$$\frac{\partial \boldsymbol{f}_p}{\partial \boldsymbol{x}}\dot{\boldsymbol{x}} + \frac{\partial \boldsymbol{f}_p}{\partial \boldsymbol{q}}\dot{\boldsymbol{q}} = 0 \tag{5}$$

or $\dot{\mathbf{x}} = \mathbf{J_p}\dot{\mathbf{q}}$, where $\mathbf{J_p} = -\mathbf{J}^{-1}_{px}\mathbf{J}_{pq}$, $\mathbf{J_{px}} = \frac{\partial \mathbf{f_p}}{\partial \mathbf{x}}$, and $\mathbf{J_{pq}} = \frac{\partial \mathbf{f_p}}{\partial \mathbf{q}} = I$. In other words, there are no forward kinematic singularities because $\mathrm{J_{pq}}$=I. Only inverse kinematic singularities exist, i.e.,$\mathbf{J}_{px} = \frac{\partial \mathbf{f_p}}{\partial \mathbf{x}} \approx 0$, where those poses possess any sufficiently small eigenvalues of $\boldsymbol{J_{px}}$.

$$\Gamma_{fp} = \{(z_m, \theta_c, \theta_a) | \boldsymbol{q} - f_{p,inv}(z_m, \theta_c, \theta_a) = 0,\ q_{\mathrm{Min}} \le q \le q_{\mathrm{Max}}\} \tag{6}$$

Γ_{fp} is shown in Fig. 3 as the red lines of a triangle, and the PKM loses the rigidity of the mechanism at these singular points.

2.3. Singularities of serial limbs

The RPS-PKM gets stuck if any of the serial limbs reach singularities. These singularities can be allocated by finding the Jacobian's singularity. Let the kinematic equation for each limb be represented by $f_{s,i}(x_i, q_i) = x - f_{s,i,fwdk}(q_i) = 0$, where $\boldsymbol{x} = \boldsymbol{f}_{s,i,fwdk}(\boldsymbol{q}_i)$ is the forward kinematics of limb i, $i = 1, \ldots 6$, $\boldsymbol{x}$ is the Cartesian coordinate of the endpoint of limb i, and $\boldsymbol{q}_i$ represents the angles of the passive joints of limb i. Taking the derivative of the kinematic equation yields:

$$\frac{\partial f_{s,i}}{\partial x_i}\dot{x} + \frac{\partial f_{s,i}}{\partial q_i}\dot{q} = 0 \tag{7}$$

or

$$\dot{\mathbf{x}}_i = \mathbf{J}_{s,i}\dot{\mathbf{q}}_i \tag{8}$$

where $\mathbf{J}_{s,i} = -\mathbf{J}^{-1}_{sx,i}\mathbf{J}_{sq,i}$, $\mathbf{J}_{\mathbf{sx},i} = \frac{\partial \mathbf{f}_{s,i}}{\partial \mathbf{x}_i} = I$ and $\mathbf{J}_{\mathbf{sq},i} = \frac{\partial \mathbf{f}_{s,i}}{\partial \mathbf{q}_i}$.

The singular configuration of the serial limb can be found when the Jacobian matrix $\boldsymbol{J_{s,i}}(Z_m, \theta_c, \theta_a)$ is singular. The equation can be described as Eq. (9)

$$\cos^2\theta_3 \sin^2\theta_3 \sin^2\theta_5 \sin\theta_6 = 0 \tag{9}$$

where $\cos\theta_3 = 0$ or $\sin\theta_3 = 0$ indicates that the PKM degenerates the motion to only translation in the vertical or horizontal direction; $\sin\theta_5 = 0$ to a planar motion; and $\sin\theta_6 = 0$ causes a self-motion of θ_5. The yellow regions in Fig. 4 demonstrate such singular regions.

These limb singular regions are not allowed inside the reachable workspace. The location of limb singularity can be removed by choosing appropriate initial angles of the ball joint of PKM.

2.4. Mechanism parameter optimization

The tool posture (z, θ_c, θ_a) is determined by the geometry dimensions of PKM, including the radius r of the moving platform, radius R of the base platform, stroke S of the limb, limits of limbs $[L_{MIN}, L_{MAX}]$ and rotational angle limit α_{MAX}. First, boundary singularities are found by:

$$\left(C_{BS}, A_{BS}, z_{BS} = \left\{(z_m, \theta_c, \theta_a) \middle| \begin{array}{c} L_{Max}=L(z_m, \theta_c, \theta_a) \| L_{Min}=L(z_m, \theta_c, \theta_a), \\ z_{Min} \le z_m \le z_{Max} \\ 0 \le \theta_c \le 2\pi \\ 0 \le \theta_a \le 0.5\pi \end{array}\right\}\right. \tag{10}$$

where (C_{BS},A_{BS},z_{BS}) represents the workspace, of which the typical shape is shown in Fig. 5. The working region of the C–A angle varies as the altitude Z changes and reaches its maximal region at an optimal altitude Z_0. The plane on this specific altitude is defined as the *optimal machining plane*.

The design procedure of the geometric parameters of the mechanism, including the three serial limbs, the connection blocks and the moving and base platforms, can be summarized as follows.

Step 1: Determine the minimal required radius r of the moving platform to mount the spindle.

Step 2: Determine the r/R and S for the maximal reachable workspace from eq. (10).

Step 3: Determine the optimal machining plane Z_0 to achieve the maximal rotational angle θ_a and θ_c. Step 4: Determine the mounting angles of the compensation blocks to remove limb singularities.

2.5. Redundancy control strategy

A redundancy control is employed once a hybrid redundant mechanism is accomplished. The 5-DOF Cartesian command $(x_m, y_m, z_m, \theta_c, \theta_a)$ was first sent to the redundancy controller, where the translational displacement in the X-, Y- and Z-axis of the SKM was used to compensate the corresponding translations of the PKM. If the translation of the PKM's effector is (x_b, y_b, z_0), then the translational outputs of

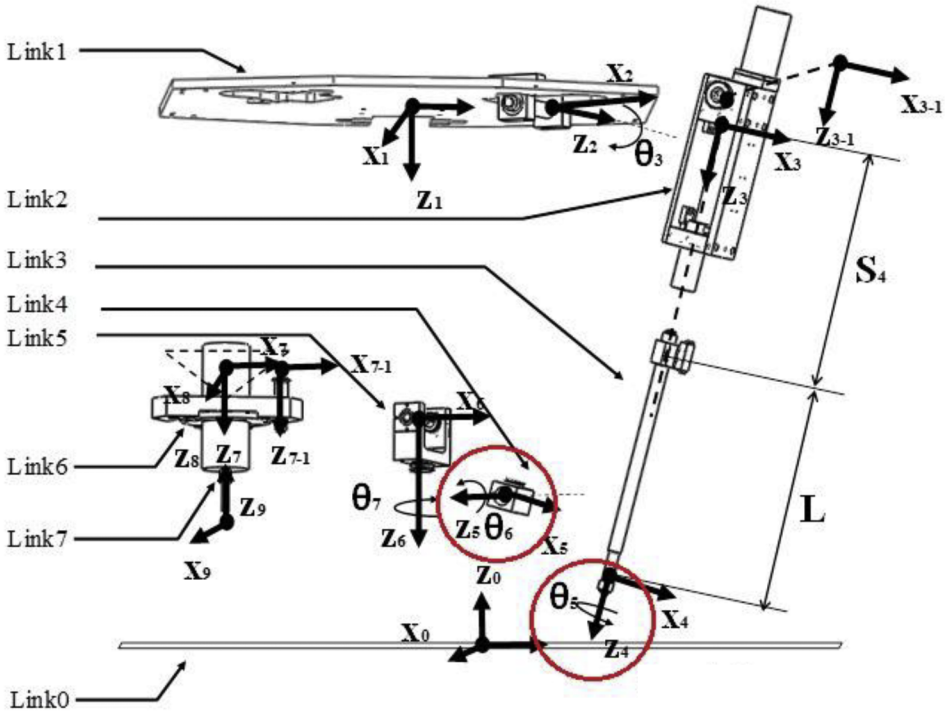

Fig. 3. Coordinate systems for forward kinematics analysis of the PKM limbs. (For interpretation of the references to colour in this figure legend, the reader is referred to the web version of this article.)

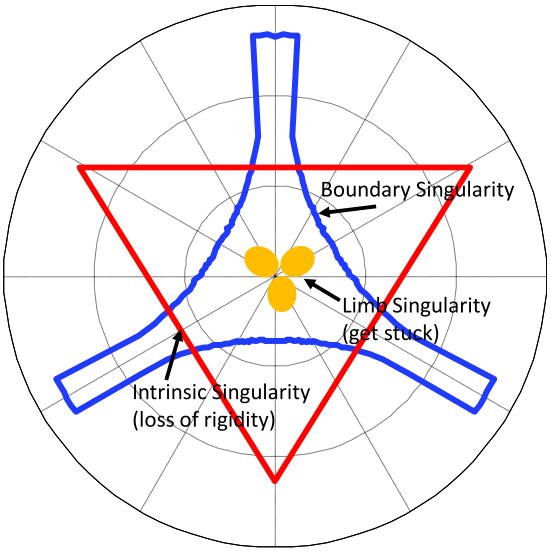

Fig. 4. Singularity classifications of the PKM.

the SKM are computed as:

$$x_w = x_m - x_t \tag{11}$$

$$y_w = y_m - y_t \tag{12}$$

$$z_w = z_m - z_0 \tag{13}$$

where x_t and y_t are the X- and Y- axis coordinates of the PKM associated with θ_c and θ_a:

$$x_t = -0.5r(c2\theta_c(c\theta a - 1) - s2\theta_c(c\theta a - 1)) \tag{14}$$

$$y_t = rc\theta cs\theta c(c\theta a - 1) \tag{15}$$

Once the Cartesian commands for the PKM and SKM have been determined, the joint command for each actuator is calculated based on the inverse kinematics for each joint controller. The overall control structure is shown in Fig. 6. where the coordinate control may be implemented by a two-degree-of-freedomH_∞feedback control, and a disturbance observer is adopted [21].

3. Results and discussions

The design optimization procedure was, first of all, to decide the spindle motor capacity and desired footprint of the machine tool. The spindle motor (ER16(36D)), Microlab Precision Inc., Taiwan) used in the prototype has an outer diameter of 80 mm. The radius r of the moving platform was chosen as 103 mm to avoid any interference between the spindle and the mounting plates of ball joints (as illustrated in Fig. 7).

The next step is to optimize the PKM's geometric dimensions so that the maximal dexterous workspace and absence of singularities can be achieved. These geometric parameters include (1) the moving vs. base platform radius ratio r/R, (2) the stroke of the linear actuator S, (3) the optimal machining plane Z_0, and (4) the mounting angle of ball joint α.

Fig. 8(a) demonstrates the simulated results of the workspace volume dependent on the r/R ratio and joint angle limits. A large workspace volume can be obtained by selecting a large joint angle limit and small r/R ratio. For example, if the joint angle limit is chosen as 90° and r/R as 0.40 as shown by the red arrow in Fig. 9(a), the workspace volume is approximately 37.5 $((\frac{R}{V})^3 \times 10^4\,\mathrm{mm}^3)$. Subsequently, the S/R ratio is required to be at least 0.53 from Fig. 8(b). In this case, the r was designed as 103 mm, and therefore the radius R of the base frame and stroke S of linear actuators were 256 mm and 136 mm, respectively. The following step is to determine the optimal machining plane $z = Z_O$ (as in Fig. 5), on which the maximal area in the rotational angles of θ_c and θ_a working space can be achieved. From the iterative algorithm, $Z_0 = 508$ mm was found, and $L_o = \sqrt{Z_o^2 + (R-r)^2} = 528.2$ mm, $L_{MAX} = L_o + \frac{1}{2}S = 596.2$ mm and $L_{MIN} = L_o - \frac{1}{2}S = 460.2$ mm could be subsequently determined. Fig. 9 shows that the rotational angle can be significantly increased from 17.5° up to 46° if the PKM can be operated on the optimal machining plane.

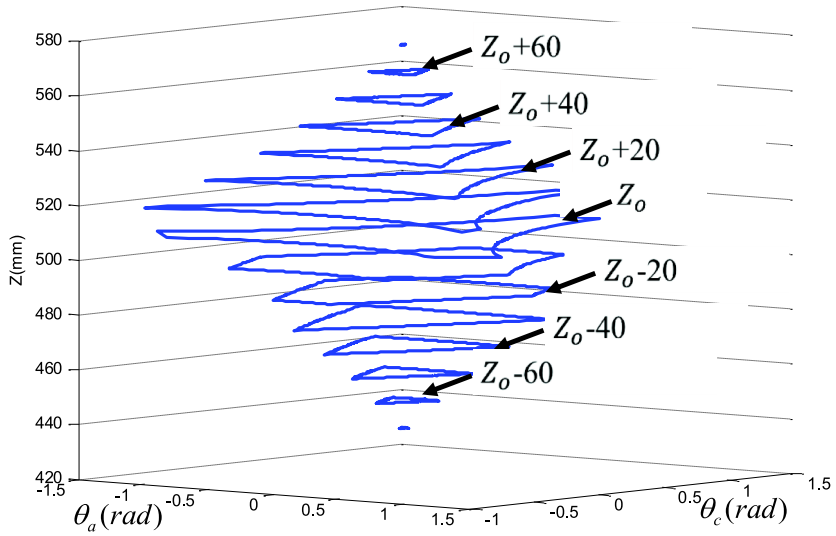

Fig. 5. Workspace of PKM and determination of the optimal plane.

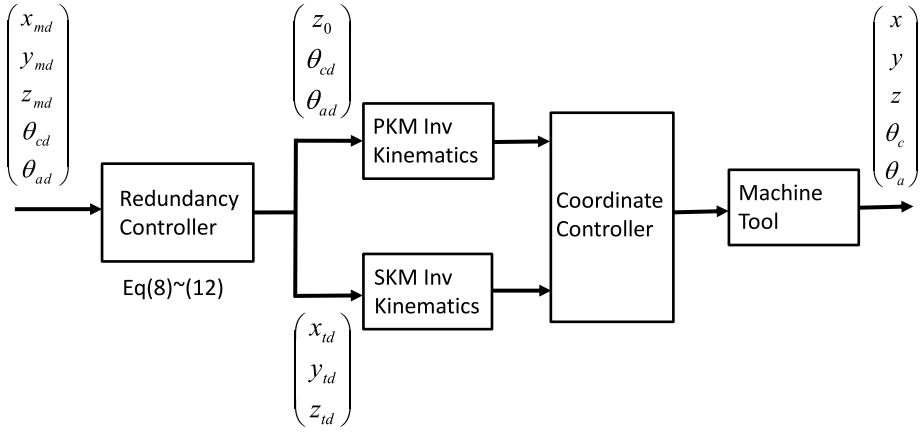

Fig. 6. Overall control structure of the redundant hybrid manipulator.

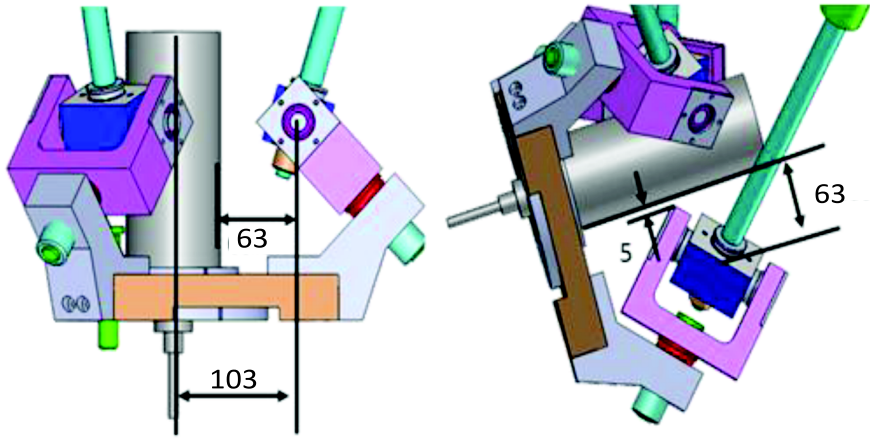

Fig. 7. Determination of the moving platform size.

3.1. Singularity removal

It is mandatory that a PKM inside its workspace be singularity-free. Otherwise, the mechanism will lose its rigidity or get stuck at these points. The derived Eqs. (6) and (7) are simulated to allocate the singularities from the mechanism and limbs. Fig. 10 shows that limb singularities occur inside the workspace if the connecting block of the limb is directly attached to the moving platform. Therefore, the rigidity of the mechanism became very poor at these regions (shown in red in Fig. 10). We observed that these singularities occur because the passive joints reached their joint limits as the end-effectors of these limbs are required to provide the calculated positions from the inverse kinematics of the PKM. Because the orientation of the end-effector is not specified from the inverse kinematics, orientation is a free vector for adjustment.

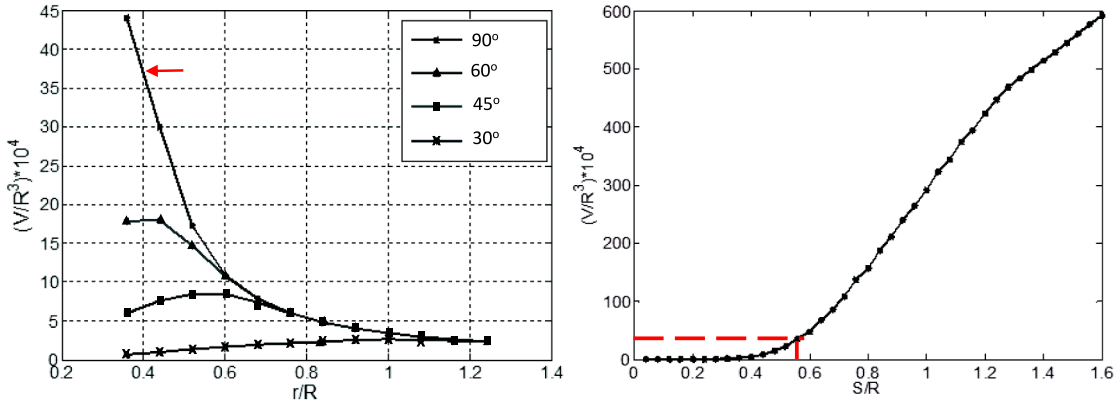

Fig. 8. (a) Workspace size vs. r/R and joint angle limit (b) workspace size vs. S/R.

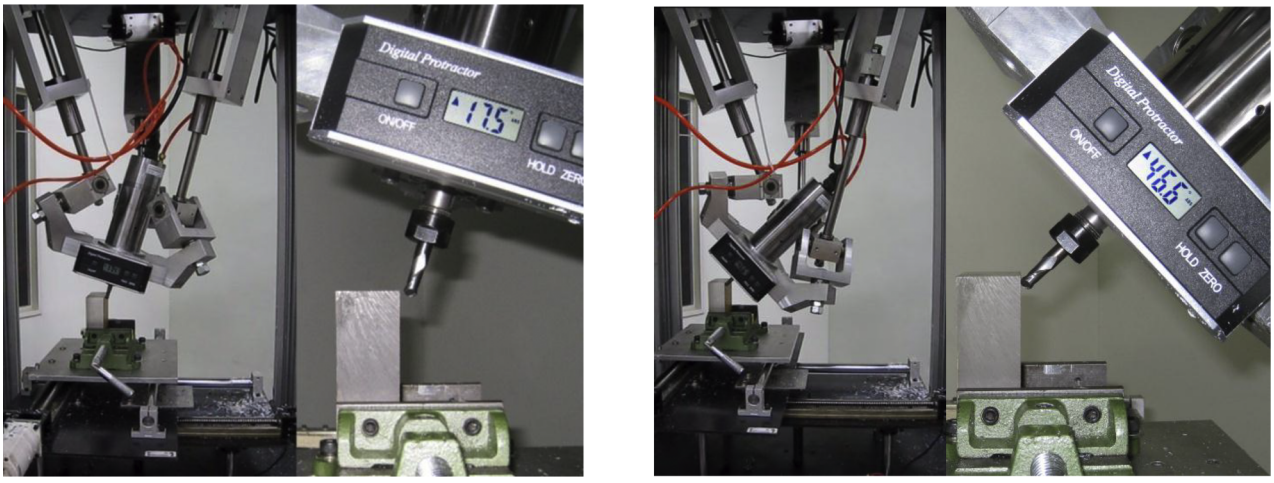

Fig. 9. Rotational angle of the tool can be increased from 17.5° to 46° when the tool tip on the parallel mechanism is constantly maintained on the optimal plane $z = 505$ mm. (For interpretation of the references to colour in the text legend, the reader is referred to the web version of this article.)

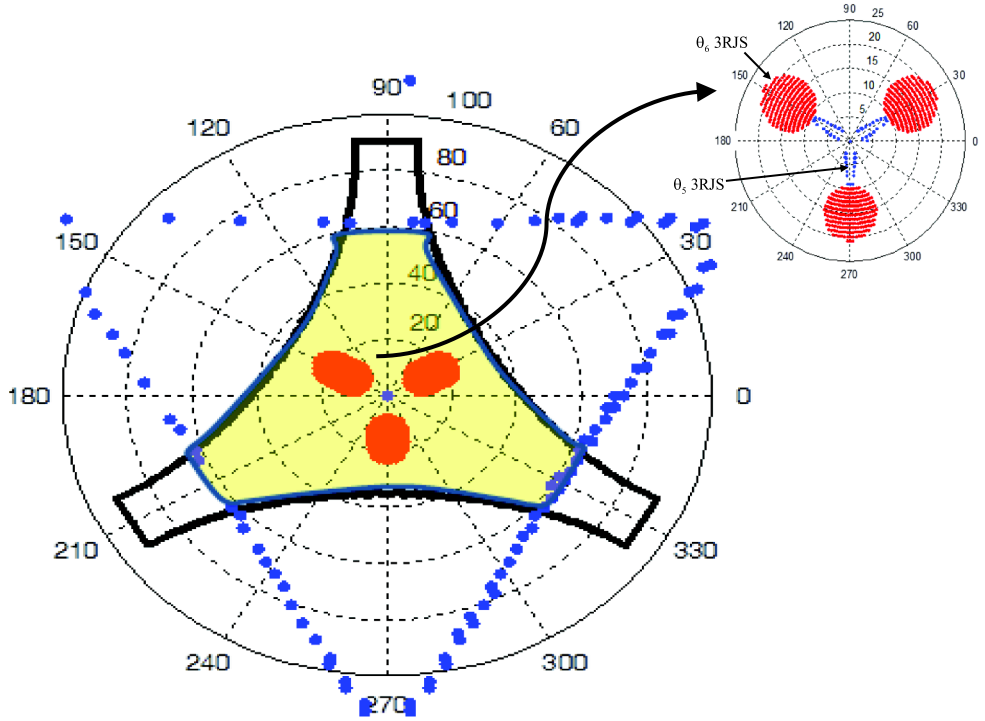

Fig. 10. Singularity analysis of the PKM: boundary singularity BS (black line), forward kinematic singularity FKS (blue line) and limb singularity RJS (red region). (For interpretation of the references to colour in this figure legend, the reader is referred to the web version of this article.)

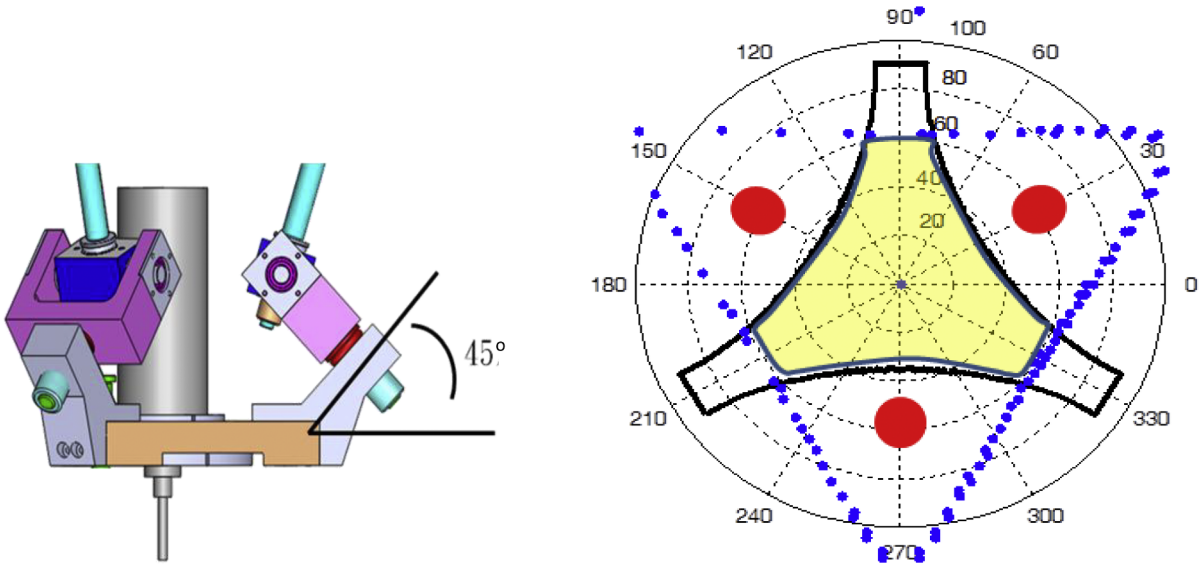

Fig. 11. (a) The compensation block with a 45° initial angle (b) the final workspace (cream-colored region) without inner singularities by introducing compensation blocks at the joints. (For interpretation of the references to colour in this figure legend, the reader is referred to the web version of this article.)

From the simulation of the orientation of the end-effector and the angles of the passive joint of these limbs, we found that these angles were within small ranges with offset angles. If we assigned the orientation of the end-effectors located near these offsets, then the limbs were able to cause any singular configuration with the workspace.

Fig. 11 shows that we assign the offset angles as -45° and attach additional compensation blocks with $-45^{\circ}$to connect the limbs and moving platform (as shown in Fig. 11(a)). Fig. 11(b) demonstrates that the singularity regions (in red) were out of the workspace (as shown in Fig. 11(b)). The iterated simulation thus enables the optimal orientation angle of the compensation block to be found so that the absence of both mechanical part interference and singularities can be met for the PKM in the entire workspace.

An experiment has also been performed to machine a knee joint implant phantom with a complex curved surface (Fig. 12). The curved surface required a spatial trajectory for which the machine tool rotated the cutter in the *A*-axis by at least 45° while simultaneously translating at least 60 mm along the *X*- and *Y*-axes and 50 mm along the *Z*-axis.

3.2. Overall evaluation of the traditional 5-axis and the proposed redundant machine

The advantages of the proposed redundancy design are two-fold. One is to shorten the required strokes of the linear actuators effectively.

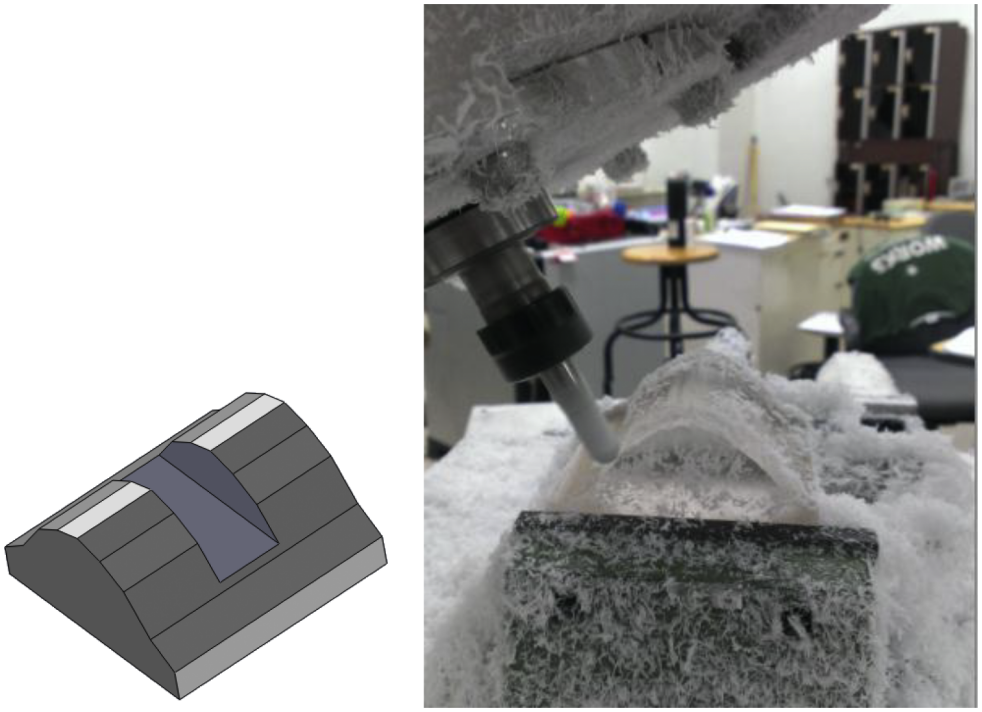

Fig. 12. Machining a customized curved surface.

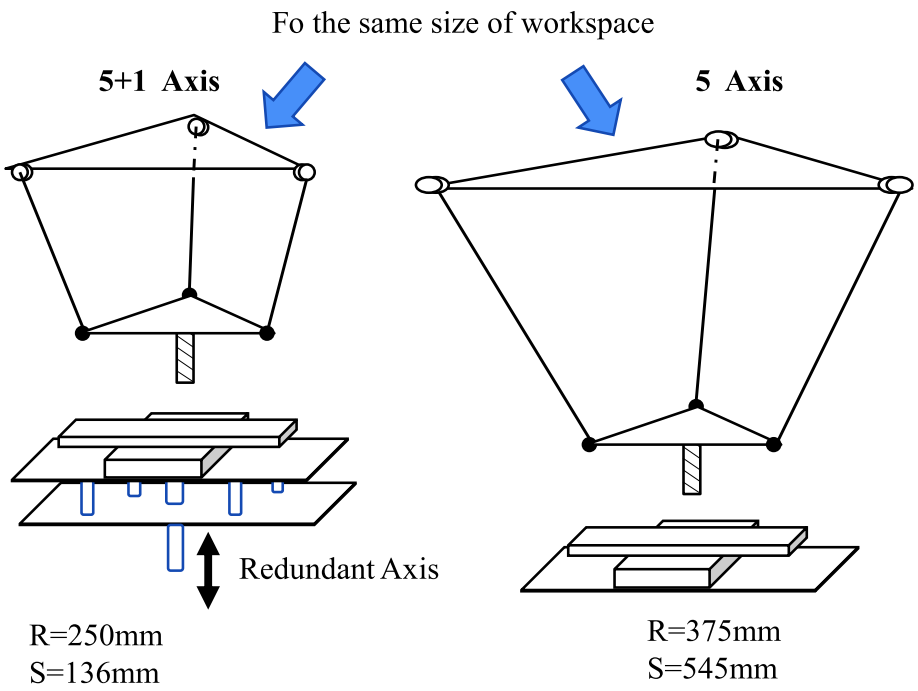

Fig. 13. Footprint comparison of a traditional PKM and the proposed redundant PKM.

This change not only improves the performance in terms of rigidity, accuracy and dynamics of the entire mechanism but also reduces the cost of material. The second is to decrease the overall machinery footprint. The small machinery footprint brings lower manufacturing cost by reducing the occupied floor space and increasing the layout flexibility of the production line. Fig. 13 shows the comparison results of the footprint under the same working space.

We simulated the dimensions for a traditional PKM to achieve the same workspace for the proposed redundant robot. The required stroke of linear actuators was calculated as 545 mm for a traditional PKM. The result shows that the stroke can be reduced by one fourth, i.e., down to 136 mm, for a linear actuator. Although an additional linear actuator is needed for the redundant *Z*-axis, the overall costs are still far less than those of the traditional counterpart. Moreover, the required diameter of the base platform calculated from the simulation was 375 mm, which was also one and a half times that of the 250 mm of the proposed redundant machine tool. Therefore, the redundancy structure produces a small volume of the PKM that enables an overall footprint that is less than that of the non-redundant counterpart.

4. Conclusion

This paper provides a systematic approach for a 5-axis machine tool to achieve a small footprint-vs.-machining-workspace ratio. A hybrid PKM and SKM with one kinematic redundancy in the *Z*-axis was proposed to set up an optimal machining plane to maximize the machining workspace and orientation angles. The compensation angles of the connecting block were appropriately adjusted to remove all limb singularities of serial limbs from the workspace of the PKM. The design concept was verified by a prototype. The results show that the machining angle can increase from 17.5° to 46.6°, while the strokes of the 3 linear actuators were reduced to only one fourth their previous value, from 545 mm to 136 mm; the diameter of base was also reduced to two thirds of the previous size, from 375 mm to 250 mm for the PKM. Therefore, the dynamic performance has high potential to be improved at the same time. In the future, dynamics characteristics will be investigated from the dynamic control perspective to compare with either its parallel or serial counterpart.

Acknowledgments

The authors would like to express their gratitude to Ministry of Science and Technology, Taiwan, for the support of the work under grant MOST 104-2221-E-002-065 and MOST 106-2218-E-002-024.

Supplementary materials

Supplementary material associated with this article can be found, in the online version, at doi:10.1016/j.rcim.2019.02.006.

References

[1] I. Fassi, G.J. Wiens, Multiaxis machining: PKMs and traditional machining centers, J. Manuf. Processes 2 (1) (2000) 1–14.
[2] P. Wenger, C. Gosselin, B. Maille, A comparative study of serial and parallel mechanism topologies for machine tools, Proc. PKM 99 (1999) 23–32.
[3] F. Xie, X.J. Liu, J. Wang, A 3-DOF parallel manufacturing module and its kinematic optimization, Rob. Comput. Integr. Manuf. 28 (3) (2012) 334–343.
[4] J. Tlusty, J. Ziegert, S. Ridgeway, Fundamental comparison of the use of serial and parallel kinematics for machines tools, CIRP Ann. Manuf. Technol. 48 (1) (1999) 351–356.
[5] V.E. Gough, S.G. Whitehall, Universal tyre test machine, Proc. FISITA 9th Int. Technical Congress, 1962, pp. 117–137.
[6] D. Stewart, A platform with six degrees of freedom, Proc. Inst. Mech. Eng. 180 (1) (1965) 371–386.
[7] M. Weck, D. Staimer, Parallel kinematic machine tools—current state and future potentials, CIRP Ann. Manuf. Technol. 51/2 (2002) 671–681.
[8] J.P. Merlet, Parallel Robots (Ed.), second ed., Structural Synthesis and Architectures, CH2 Springer Publishing Company, 2010, pp. 19–93.
[9] K. Harib, K.A.F. Moustafa, A.M.M. Sharif Ullah, S. Zenieh, Parallel, serial and hybrid machine tools and robotics structures: comparative study on optimum kinematic design, in: S. Kucuk (Ed.), Serial and Parallel Robot Manipulators: Kinematic Dynamics and Control, 2012 ISBN 979-953- 307-550-0109-123.
[10] X.J. Liu, X. Tang, J. Wang, A novel 2-DOF parallel mechanism based design of a new 5-axis hybrid machine tool, Proc. of IEEE Int. Conf. on Rob. and Auto. 2003, pp. 3990–3995.
[11] D. Pisla, B. Gherman, C. Vaida, M. Suciu, N. Plitea, An active hybrid parallel robot for minimally invasive surgery, Rob. Comput. Integr. Manuf. 29 (2013) 203–221.
[12] K.C. Fan, H. Wang, J.W. Zhao, T.H. Chang, Sensitivity analysis of the 3-PRS parallel kinematic spindle platform of a serial-parallel machine tool, Int. J. Mach. Tools Manuf. 43 (15) (2003) 1561–1569.
[13] J.V. Fontes, M.M. da Silva, On the dynamic performance of parallel kinematic manipulators with actuation and kinematic redundancies, Mech. Mach. Theory 103 (2016) 148–166.

[14] J. Wu, J. Wang, L. Wang, T. Li, Z. You, Study on the stiffness of a 5-DOF hybrid machine tool with actuation redundancy, Mech. Mach. Theory 44 (2009) 289–305.
[15] F. Xie, X.J. Liu, Y. Zhou, Development and experimental study of a redundant hybrid machine with five-face milling capability in one setup, Int. J. Precis. Eng. Manuf. 15 (1) (2014) 13–21.
[16] C. Gosselin, T. Laliberte, Singularity-free kinematically redundant planar parallel mechanisms with unlimited rotational capability, IEEE Trans. Rob. 31 (2) (2015) 457–467.
[17] M. Isaksson, Kinematically redundant planar parallel mechanisms for optimal singularity avoidance, J. Mech. Des. 139 (4) (2017) 042302-042302-9.
[18] A.G. Ruiz, J.C. Santos, J. Croes, W. Desmet, M.M. da Silva, On redundancy resolution and energy consumption of kinematically redundant planar parallel manipulators, Robotica 36 (6) (2018) 809–821.
[19] S. Li, J. He, Y. Li, M.U. Rafique, Distributed recurrent neural networks for cooperative control of manipulators: a game-theoretic perspective, IEEE Trans. Neural Netw. Learn. Syst. 28 (2) (2017) 415–426.
[20] A.M. Mohammed, S. Li, Dynamic neural networks for kinematic redundancy resolution of parallel stewart platforms, IEEE Trans. Cybern. 46 (7) (2016) 1538–1550.
[21] P.L. Yen, A two-loop robust controller for compensation of the variant friction force in an over-constrained parallel kinematic machine, Int. J. Mach. Tools Manuf. 48 (2008) 1354–1365.